Received: 26 December 2022 | Accepted: 28 December 2022

DOI: 10.1002/jcu.23423

REVIEW

WILEY

Second trimester fetal MRI of the brain: Through the ground glass

Nevena Fileva[1] | Mariasavina Severino[2] | Domenico Tortora[2] | Antonia Ramaglia[2] | Dario Paladini[3] | Andrea Rossi[2,4]

[1]Department of Radiology, Medical University of Sofia, Sofia, Bulgaria

[2]Neuroradiology Unit, IRCCS Istituto Giannina Gaslini, Genoa, Italy

[3]Fetal Medicine and Surgery Unit, IRCCS Istituto Giannina Gaslini, Genoa, Italy

[4]Department of Health Sciences (DISSAL), University of Genoa, Genoa, Italy

Correspondence
Andrea Rossi, Neuroradiology Unit, IRCCS Istituto Giannina Gaslini, Via Gerolamo Gaslini 5, 16147 Genoa, Italy.
Email: andrearossi@gaslini.org

Abstract

Fetal MRI is an important tool for the prenatal diagnosis of brain malformations and is often requested after second-trimester ultrasonography reveals a possible abnormality. Despite the immature state of the fetal brain at this early stage, early suggestive signs of the presence of brain malformations can be recognized. To differentiate between the normal dynamics of the growing brain and the developing pathological conditions can be challenging and requires extensive knowledge of normal central nervous system developmental stages and their neuroradiological counterparts at those different stages. This article reviews the second-trimester appearances of some commonly encountered brain malformations, focusing on helpful tricks and subtle signs to aid in the diagnosis of such conditions as rhombencephalosynapsis, various causes of vermian rotation, molar tooth spectrum anomalies, diencephalic-mesencephalic junction dysplasia, ganglionic eminence anomalies, and the most common malformations of cortical development.

KEYWORDS
brain malformations, cortical malformation, fetal brain MRI, posterior fossa

1 | INTRODUCTION

Ultrasound is a cornerstone of fetal morphology assessment and is typically obtained between the 19th and 21st gestational weeks (GW). In case of doubtful findings, fetal MRI can provide key information to confirm or reject the suspected pathology. Due to the immature stage of development, however, normal structures have a quite different appearance compared to the postnatal period. The combination of an immature brain and the rudimentary, not "textbook" appearance of abnormalities can make the diagnosis highly challenging.

Policies for voluntary termination of pregnancy vary around the world. Comparing the laws in 158 different countries, the results showed that in 1 of 3 of them, abortion at a woman's request is allowed until 12 weeks of pregnancy. Furthermore, there are lists of reasons regarding the health of the woman or the fetus that can indicate the need for termination of the pregnancy. In half of the included countries, abortion due to fetal conditions is allowed within a median gestational age of 22 weeks, varying between 8 and 35 GW.[1] The age limits for this important decision may result into additional pressure on the neuroradiologist for an early diagnosis in cases of suspected brain malformations. Several patients are sent for a fetal MRI soon after the screening US at the end of the second trimester, that is, at 20–22 GW. A follow-up exam later in pregnancy (typically at 28–30 weeks) is frequently recommended but may not be feasible or when an earlier limit for pregnancy termination exists.

Interpretation of fetal brain MRI can be challenging due to the rapidly dynamic changes occurring in the developing structures. Some imaging findings can be normal at certain ages and abnormal at others. Understanding the embryology and the normal appearance at each gestational age is critical for detecting potential pathologies. Using standard measurement charts is an important aspect of the

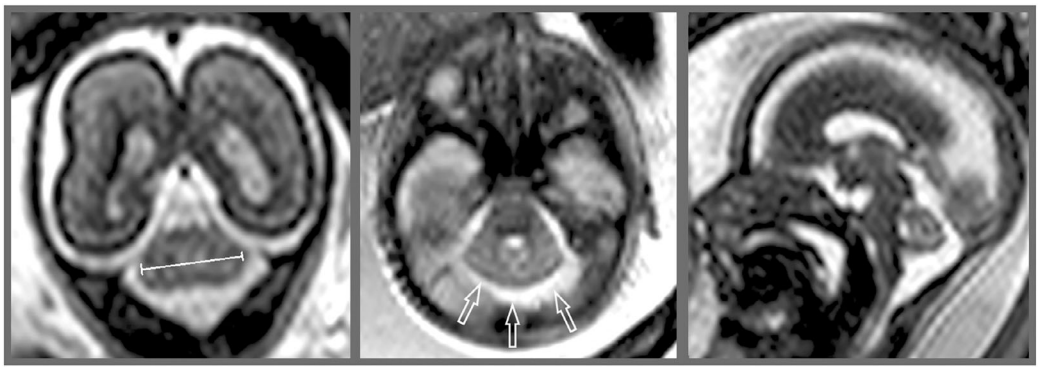

FIGURE 1 Rhombencephalosynapsis at 22 GW. (A) coronal T2-weighted image shows decreased transverse cerebellar diameter (line); (B) axial T2-weighted image shows convexity of the posterior cerebellar margin (arrows) due to absence of the vermis and vallecula; this feature, together with the abrupt angulation between the lateral and posterior cerebellar margins, generates a typical "bell-like" shape of the single-lobed cerebellum. (C) sagittal T2-weighted image shows absence of the primary fissure of the vermis, which should normally be visualized at this gestational age

FIGURE 2 Rhombencephalosynapsis and ventriculomegaly at 21 GW. (A) Coronal T2-weighted image shows decreased transverse cerebellar diameter (line) and severe ventriculomegaly; (B) sagittal T2-weighted image suggests aqueductal stenosis (arrow) and also fails to visualize a normal primary vermian fissure; (C) axial T2-weighted image shows bell-shaped, fetus with combined brain malformations; the imaging findings referring to the RES (A–C) including the reduced transverse cerebellar diameter, the bell-like shape of the single-lobed cerebellum with rudimentary vallecula, suggestive of partially RES (black arrow); mesencephalic abnormality (B/D) presented with dysmorphic brainstem in sagittal plane secondary to aqueductal stenosis (white arrow) leading to hydrocephalus and heart-shaped mesencephalon due to the lack of separation called mesencephalosynapsis (white circle)

exam evaluation[2,3] and can be greatly helpful to recognize subtle abnormalities. While a description of the technical issues, protocols, and parameters for fetal brain MR imaging is beyond the scope of this article, it is important to underscore that a robust acquisition technique, centered onto triplanar single-shot echo planar T2-weighted sequences but also including other sequences such as T1-weighted, susceptibility-weighted, FLAIR, and others in conditions of sufficient fetal immobility and maternal comfort is of paramount importance to successfully perform and correctly interpret these imaging studies.

2 | RHOMBENCEPHALOSYNAPSIS

Rhombencephalosynapsis (RES) is a rare malformation characterized by fusion of the cerebellar hemispheres with vermian aplasia and hypoplasia (total or partial). The genetic basis is still unknown, and the majority of cases are presumed to be sporadic and related to de novo dominant mutations.[4] Cerebellar development begins around the 6th gestational week with the proliferation of neuroblasts at the rhombomere 1 (R1 segment) of the anterior hindbrain; RES is presumed to be consistent with a defect arising early thereafter.[5,6] Patients with RES can present with a variety of clinical symptoms and neurodevelopmental outcomes; while the malformation can rarely be an incidental finding in otherwise normal individuals, more frequently it is part of complex syndromes (VACTERL-RES, Gomez-Lopez-Hernandez, and others) with severe neurological impairment.[4]

Diagnostic findings in RES in the mature and postnatal brain include vermian absence (complete or partial), fusion of the cerebellar hemispheres with a transverse orientation of the inferior cerebellar foliation ("sandwich" appearance), fusion of the dentate nuclei and superior cerebellar peduncles, and absence of the vermian primary fissure.[7] However, in the fetal brain these structures are still developing, and such signs may not be so prominently displayed. RES should be suspected and ruled out in every fetus with a reduction of the transverse cerebellar diameter (TCD below the third centile). In the axial plane, an abrupt change in orientation between the lateral and posterior aspects of the cerebellum is visualized; its combination with vallecular flattening or absence results in a specific bell-like (or round) shape of the single-lobed cerebellum[4] (Figiures 1 and 2).

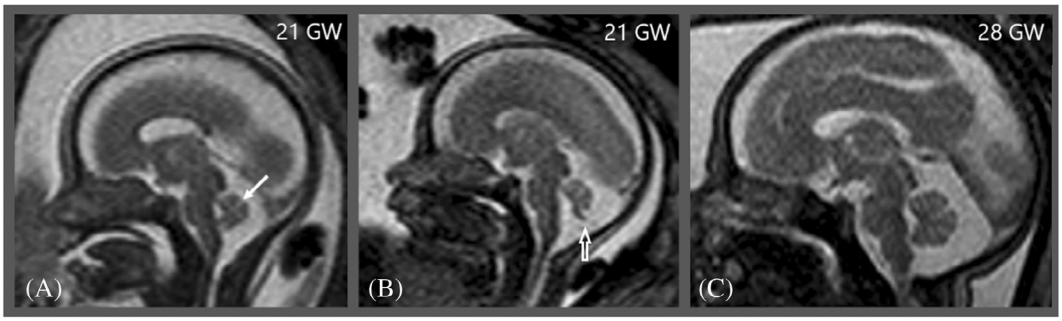

FIGURE 3 Second trimester appearances of the posterior fossa (A) sagittal T2-weighted image in a normal fetus at 21 GW shows that, as expected, the vermis has closed the fourth ventricle. Notice primary fissure (arrow); (B) sagittal T2-weighted image in another 21 GW fetus shows rotated vermis with normal size for the gestational age with wide communication between the fourth ventricle and the cisterna magna; notice the cerebellar tail sign (white arrow); (C) At 28 GW, sagittal T2-weighted image in the same fetus as B reveals completed rotation of the vermis and normal posterior fossa appearance

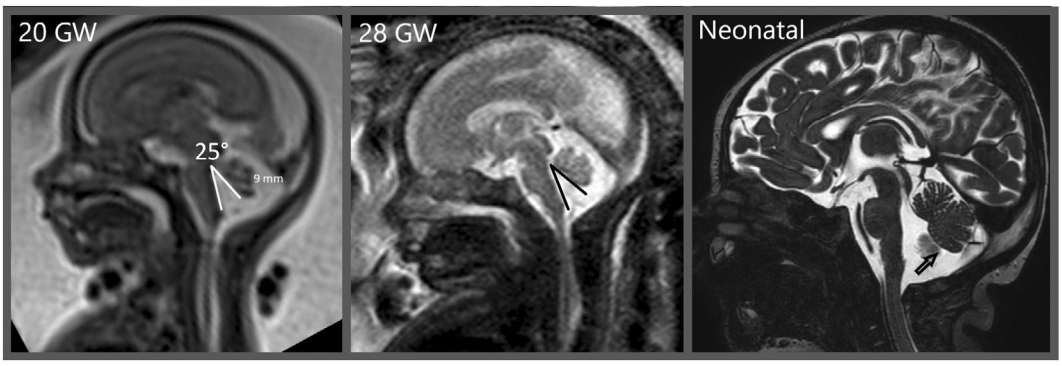

FIGURE 4 Blake's pouch cyst. (A) Sagittal T2-weighted image at 20 GW shows predictive criteria for incomplete vermian rotation, including a brainstem-vermis angle ≥23°, width of the cisterna magna ≥9 mm and the presence of the "cerebellar tail sign"; (B) follow-up exam at 28 GW shows the persistence of an enlarged brainstem-vermis angle; (C) Sagittal T2-weighted image obtained postnatally confirms rotated vermis with inferior hypoplasia (arrow)

RES is often part of complex malformation syndromes, including anomalies in the pons, midbrain, and forebrain associated with ventriculomegaly.[8] The accompanying hydrocephalus may be secondary to aqueductal stenosis, often resulting from median fusion of the midbrain, or mesencephalosynapsis. Enlarged ventricles are often the first noticeable sign of a brain abnormality, prompting the MR examination; thus, specific attention to cerebellar morphology should be given in all cases with ventriculomegaly. Partial RES poses a big diagnostic challenge due to the absence of clear clues and requires a high level of suspicion and a careful analysis of the cerebellar anatomy.[4]

3 | VERMIAN ROTATION

The cerebellum originates from rhombomere 1, a primordium arising from the isthmus (junction between the primitive mesencephalon and rhombencephalon) and growing into the rhombencephalic vesicle. Normal vermian development begins in the anterior membranous area of the primitive rhombencephalic vesicle, with a direct proliferation of the mesial primordium forming the vermis in the ventrodorsal direction.[9] The plica choroidea originates the choroid plexus of the fourth ventricle and separates the anterior and posterior membranous areas.[10] The latter is an inferior portion of the

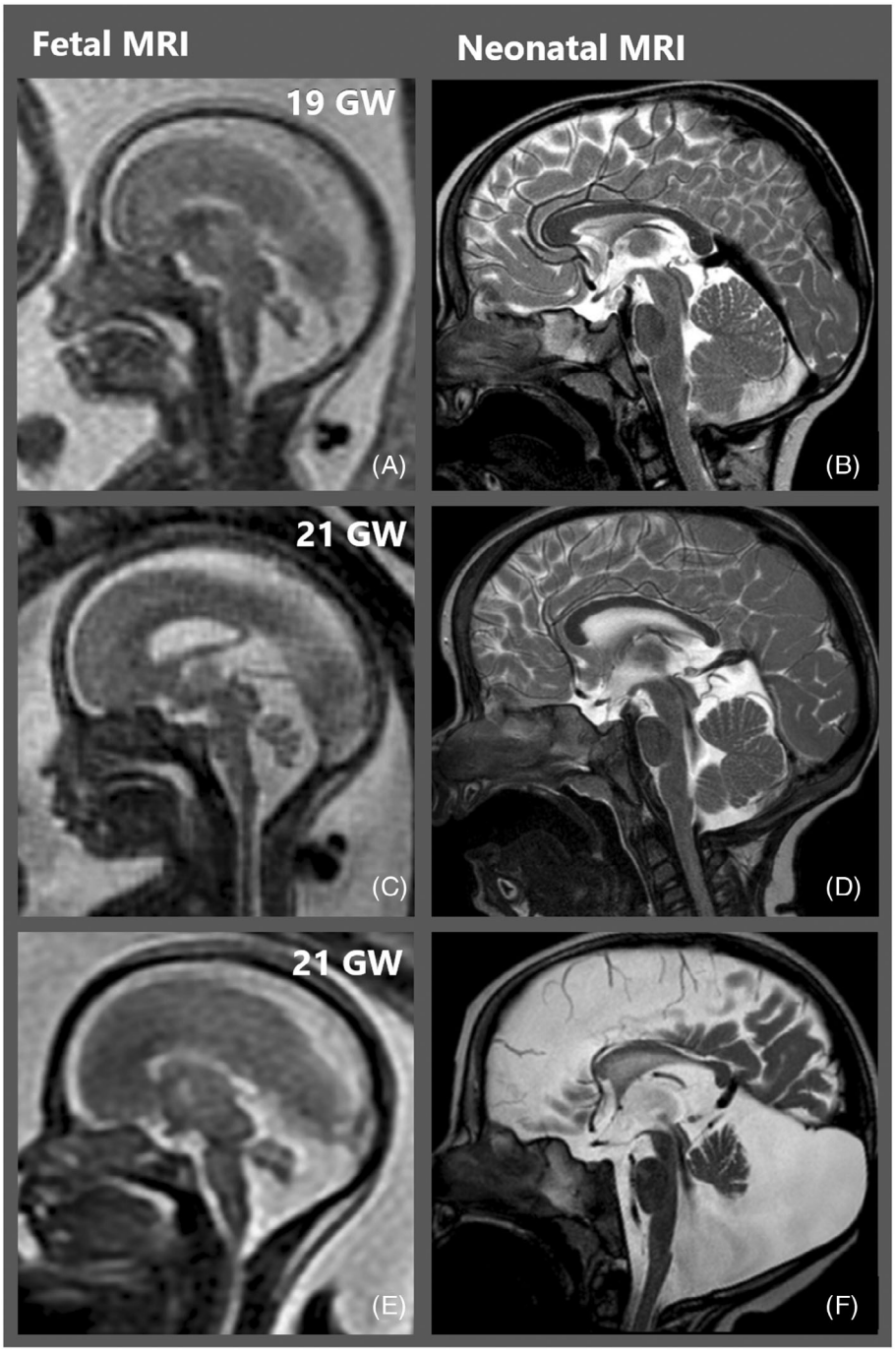

FIGURE 5 Corresponding images of fetal and postnatal MRI in three patients with vermian rotation. All fetal sagittal T2-weighted MR images (A, C, E) were obtained at 19–21 GW and show similar features, consisting of incomplete rotation of the vermis and wide communication between the fourth ventricle and the cisterna magna. Patient 1 (A, B) is demonstrative of delayed vermian rotation with normal postnatal exam; Patient 2 (C, D) is consistent with a persistence of the Blake's pouch with ensuing vermian hypoplasia; Patient 3 (E, F) demonstrates evolution into a full-blown Dandy-Walker malformation, with progressive enlargement of the posterior fossa and counter-clockwise rotation of the hypoplastic vermis

fourth ventricular roof which progressively disappears during development, through a phase of outpouching (the so-called Blake's pouch) and permeabilization. This process is usually completed at 20 GW, so that the vermis is already visible in its normal position with an acute fastigium and a small foramen of Magendie (Figure 3). However, this process can be delayed or interrupted in some cases, resulting in a persistence of the pouch, also called *Blake's pouch cyst* (BPC)[11] (Figure 4). Research by Paladini et al. reported that greater than 50% of cases of initially persistent BPC eventually have the fenestration process completed between 24 and 26 GW.[12]

Vermian hypoplasia (VH) is characterized by a reduced size of the vermian structure (most often involving the inferior portion) and can be associated with upward rotation without enlargement of the posterior fossa. Isolated hypoplasia is reported to have a favorable prognosis in 75% of patients.[13] The *Dandy-Walker malformation* (DWM) is a cystic enlargement of the fourth ventricle with a hypoplastic and aplastic vermis that is rotated counter-clockwise and may be associated with cerebellar hypoplasia, hydrocephalus, and other commissural or cortical abnormalities.[7] Whether tentorial and torcular elevation with posterior fossa enlargement are necessary components of the DWM constellation of findings is presently disputed; recent research proposes that they are per se insufficiently specific in distinguishing DWM, VH, and BPC.[14]

Establishing predictive criteria for the future development of the cerebellar structures has been a major focus of recent research. Importantly, BPC, VH, and DWM can all lead to an increased amount of fluid in the posterior fossa and may have similar radiological features during the second trimester of gestation,[13] including a wide communication between the fourth ventricle and the cisterna magna[11] (Figure 5). In fetuses at 26 GW or younger, the presence of ≥2 factors: (i) a brainstem-to-vermis angle ≥23°; (ii) width of the cisterna magna ≥9 mm; and (iii) presence of the "cerebellar tail sign" have been shown to have a sensitivity of 84.21% (95% CI, 60.4%–96.6%) and specificity of 80.8% (95% CI, 60.6%–93.4%) in predicting the persistence of vermian rotation at imaging follow-up.[15] Although an increased brainstem-vermis angle is associated with a higher risk of vermian rotation, its persistence when isolated should not be used as a specific marker for malformation and developmental delay; importantly, cases of larger brainstem-to-vermis angulation (28° at 21 GW and 43° at 19 GW) have been reported in which follow-up examinations revealed normalized anatomy.[11]

The posterior-to-anterior vermis ratio is another useful differentiation criterion; values below 2:1 are suggestive of DWM or VH. In one study, this criterion showed greater specificity in excluding BPC rather than the width of the brainstem-vermis angle.[16]

The cerebellar tail sign represents a dysplastic thickening of the fourth ventricle roof, possibly containing a displaced cerebellar germinal matrix. It was previously thought to be strongly suggestive of DWM, but it has also been demonstrated in BPC,

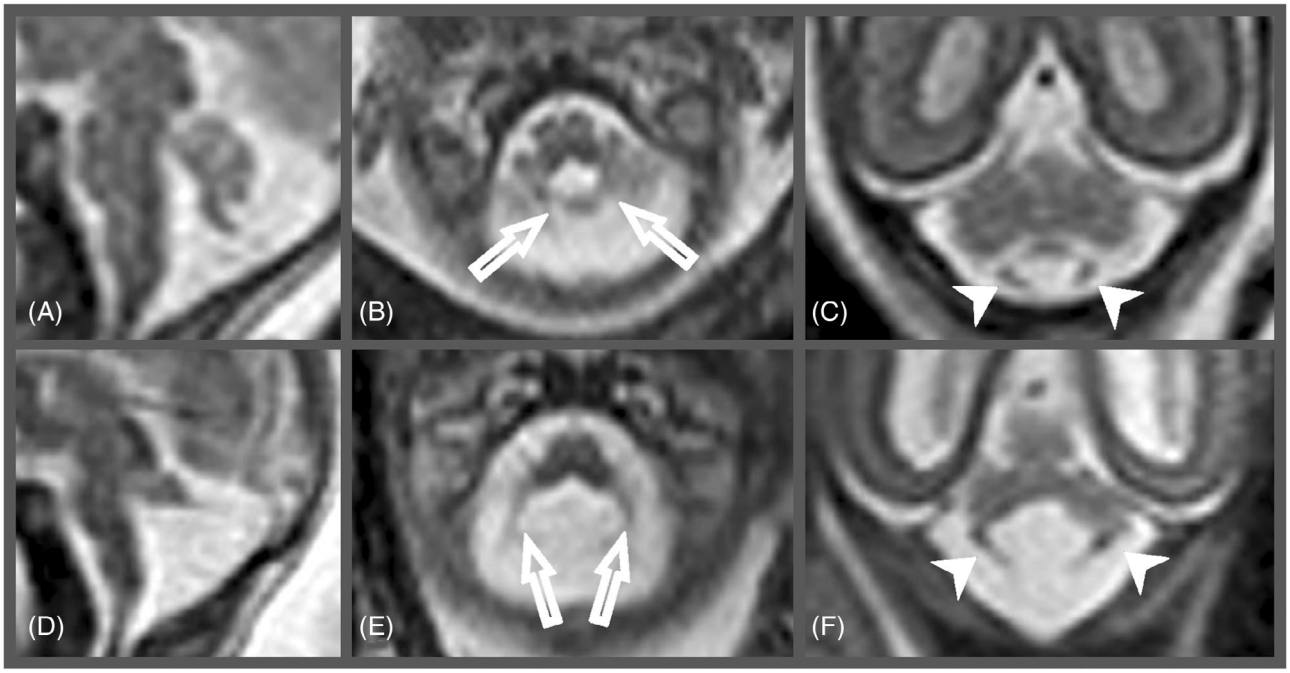

FIGURE 6 The taenia-tela choroidea complex in posterior fossa abnormalities. (A–C) Blake's pouch cyst at 21 GW. (A) sagittal T2-weighted image shows rotated vermis and cerebellar tail sign; (B) axial and (C) coronal T2-weighted images show median location of taenia–tela choroidea complex that tends to connect to the inferior vermis (arrows, B) and fourth ventricular choroid plexus above the anterior and inferior vermian margin (arrowheads C). (D–F) Dandy-Walker malformation at 21 GW. (A) Sagittal T2-weighted images shows classical counter-clockwise rotation of a hypoplastic vermis, forming a 70° brainstem-vermis angle; (E) axial and (F) coronal T2-weighted images show taenia–tela choroidea complex is spread out deviating from the midline and the vermis (arrows, E), as well as inferolateral location of the choroid plexus along the wall of the fourth ventricle (arrowheads, F)

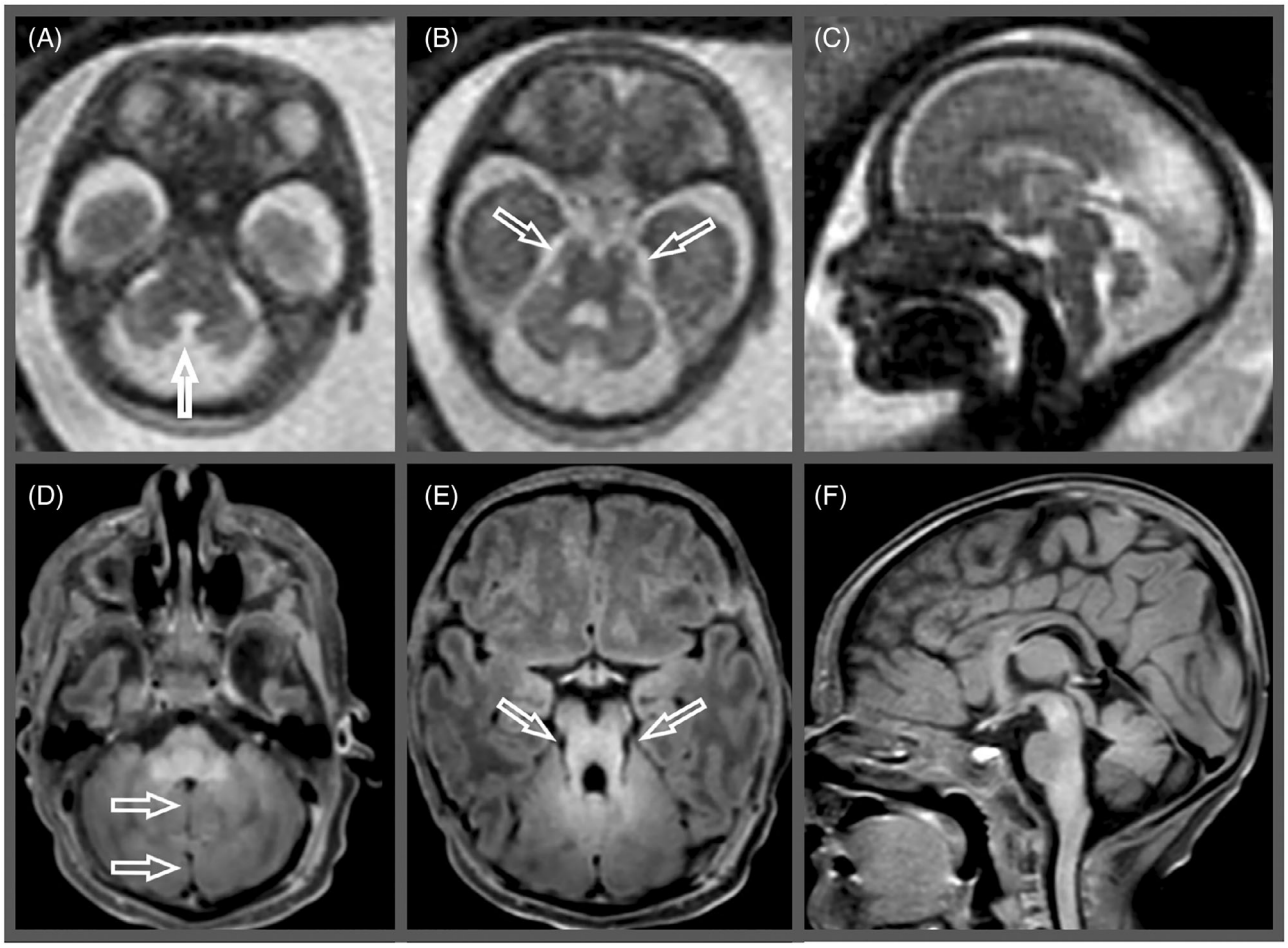

FIGURE 7 Molar tooth sign. (A–C) Fetal MRI at 21 GW and (D–F) corresponding neonatal MRI (D/E/F) in a patient diagnosed with Joubert syndrome. (A) and (B) axial T2-weighted images show hypoplasia of the vermis with large communication between the fourth ventricle and cisterna magna (arrow, A) and subtle molar tooth sign (axial, B); (C) sagittal T2-weighted image shows mildly hypoplastic vermis. Postnatally, there is evidence of hypoplasia of the inferior cerebellar vermis with a midline cleft (arrows, D) and thickened and elongated superior cerebellar peduncles forming the "molar tooth" appearance in the axial plane (arrows, E). Notice mildly hypoplastic vermis with coarse foliation (F).

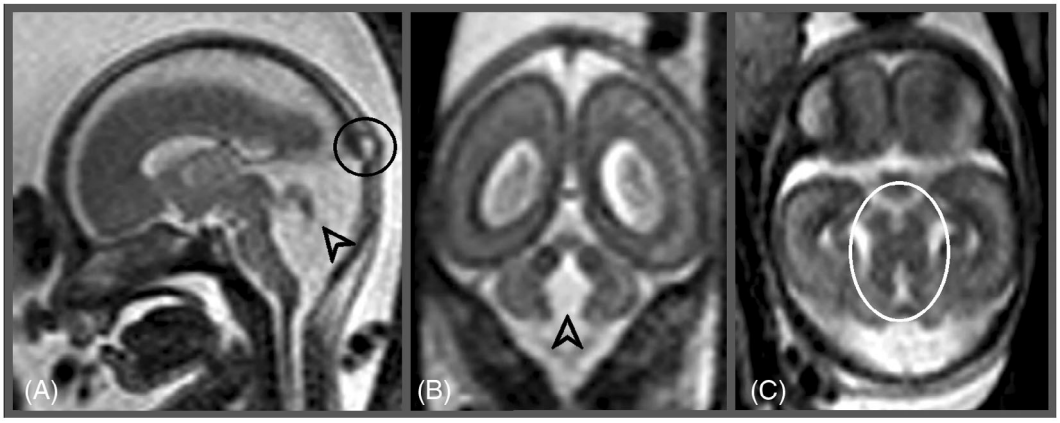

FIGURE 8 Molar tooth sign at 21 GW. (A) Sagittal T2-weighted image shows dysmorphic, hypoplastic vermis (arrowhead) and concurrent occipital meningocele (black circle). (B) coronal T2-weighted image shows wide communication between the fourth ventricle and cisterna magna (arrowhead). (C) Axial T2-weighted image shows typical "molar tooth" appearance (white circle)

especially in younger fetuses with a tail-like choroid plexus and distorted vermian tissue.[15] According to recent research, the cerebellar tail sign is not per se sufficient to differentiate between DWM and BPC.[16]

The locations of the choroid plexus of the fourth ventricle and the taenia–tela choroidea complex, and the angles they form, have been shown to vary significantly among normal, BPC, and DWM and VH exams (Figure 6). Based on the current understanding of embryological development that categorizes cystic posterior fossa malformations into those pertaining to the anterior (DWM and VH) and posterior membranous areas (BPC) respectively,[10] displacement of the choroid plexus and taenia-tela choroidea complex can be expected to vary. Specifically, a medial location of the taenia–tela choroidea complex and a choroid plexus located above the anterior and inferior vermian margin is seen in normal fetuses and in cases of BPC; conversely, an inferolateral location of the choroid plexus along the wall of the fourth ventricle, with the taenia–tela choroidea complex displaced distantly from the vermian margin, are seen in those with DWM and VH.[16]

4 | MOLAR TOOTH SIGN

Primary nonmotile ciliopathies are characterized by dysregulation of several embryological development pathways affecting the kidneys, brain, retina, liver, pancreas, and skeletal system. There are more than 50 different gene mutations identified, leading to a wide range of clinical presentations, ranging from the classical Joubert phenotype (characterized by developmental delay, hypotonia, oculomotor apraxia, and breathing difficulties) to complex syndromes.[17]

On imaging, there is a pathognomonic "molar tooth sign", generated by absent decussation of the superior cerebellar peduncles in the midbrain, resulting into horizontally oriented, thickened, and elongated superior cerebellar peduncles which are combined with an abnormally deep interpeduncular fossa; a wide range of vermian hypoplasia with deranged foliation is associated.[18] On fetal MRI, the appearance of the superior cerebellar peduncles needs to be carefully evaluated in all cases of vermian hypoplasia (Figures 7 and 8). The molar tooth sign will often appear on a single axial image and can be altogether missed if the axial orientation of the slices is not at the proper angulation (Figure 9).

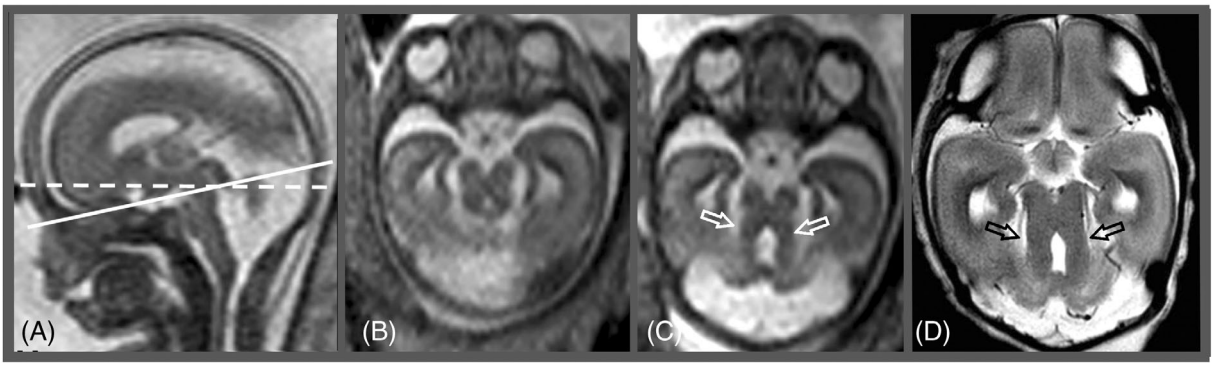

FIGURE 9 Molar tooth sign, 20 GW. (A) Sagittal T2-weighted image showing hypo-dysplastic vermis and wide communication between the fourth ventricle and the cisterna magna; (B) axial T2-weighted image (plane indicated by the solid line on A) shows misleading, relatively normal appearance of the midbrain; (C) axial T2-weighted image with different angulation (dotted line on A) reveals classical molar tooth sign (arrows), which is confirmed on post-mortem imaging (arrows, D)

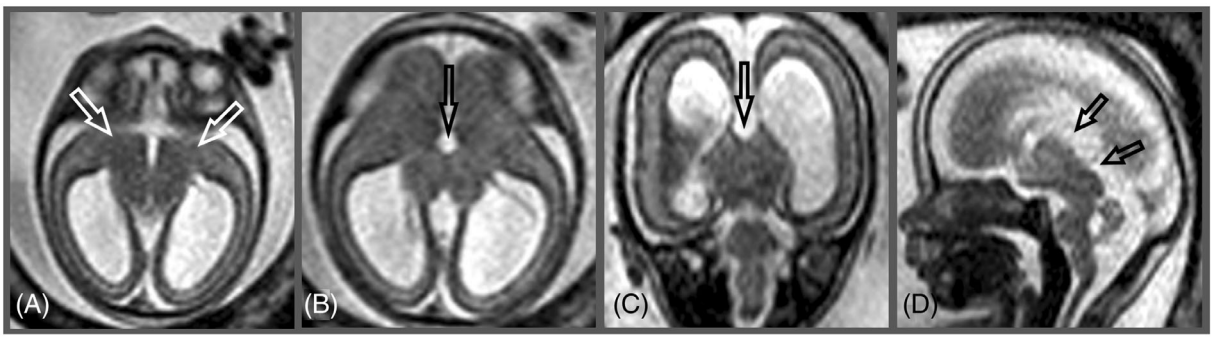

FIGURE 10 Diencephalic-mesencephalic junction dysplasia in a 21 GW fetus with partial corpus callosum agenesis and L1 syndrome. (A) Axial T2-weighted image shows enlarged dorsoventral size of the brainstem and abnormal midbrain contour in the axial plane, with ventral cleft, forming the butterfly sign (white arrows). (B) axial and (C) coronal T2-weighted images show midline fusion of the thalami, or diencephalosynapsis (arrow), ventriculomegaly, and corpus callosum agenesis; (D) sagittal T2-weighted image shows lack of separation between the massa intermedia of the thalamus and the midbrain (arrows)

Its recognition can be challenging, but it should be carefully looked for and excluded especially in suspected cases where there is a positive family history, associated kidney anomalies, polydactyly, cleft lip, and hypothalamic hamartoma.[19]

5 | DIENCEPHALIC-MESENCEPHALIC JUNCTION DYSPLASIA

Diencephalic-mesencephalic junction dysplasia (DMJD) is a malformation feature characterized by a developmental lack of cleavage between the diencephalon and the midbrain. It is categorized into two groups: (i) type A shows an enlarged dorsoventral size of the brainstem and abnormal midbrain contour in the axial plane, with or without ventral cleft (the butterfly sign), indicating a lack of separation between the thalamus and the midbrain; (ii) type B is recognized better in the sagittal plane and is characterized by a lack of separation between the massa intermedia of the thalamus and the upper aspect of the midbrain[20]

In fetal evaluation (Figure 10), obstructive ventriculomegaly is usually the first alarming sign that prompts further examinations. It is reported that the specific "butterfly sign" of the midbrain can be recognized as early as 20–21 GW. Again, the correct angulation of the axial slices is crucial in those cases.[21]

L1 is one of the syndromes associated with DMJD that can be suggested by means of fetal MRI. It is an X-linked developmental disorder due to L1CAM mutations, characterized by hydrocephalus of varying degrees of severity, intellectual deficit, spasticity of the legs, and adducted thumbs. The MRI findings include DMJD variably associated with diencephalosynapsis (lack of separation between the two thalami visualized as a large massa intermedia without a cleavage), ventriculomegaly, and corpus callosum agenesis.[22] Recognition of adducted thumbs is also possible on fetal MRI.

6 | GANGLIONIC EMINENCE ABNORMALITIES

The ganglionic eminences (GE) are located next to the lateral ventricles in the ventral telencephalon bilaterally. The progenitor neuronal cells in the GE give rise to the basal ganglia and will produce a wide

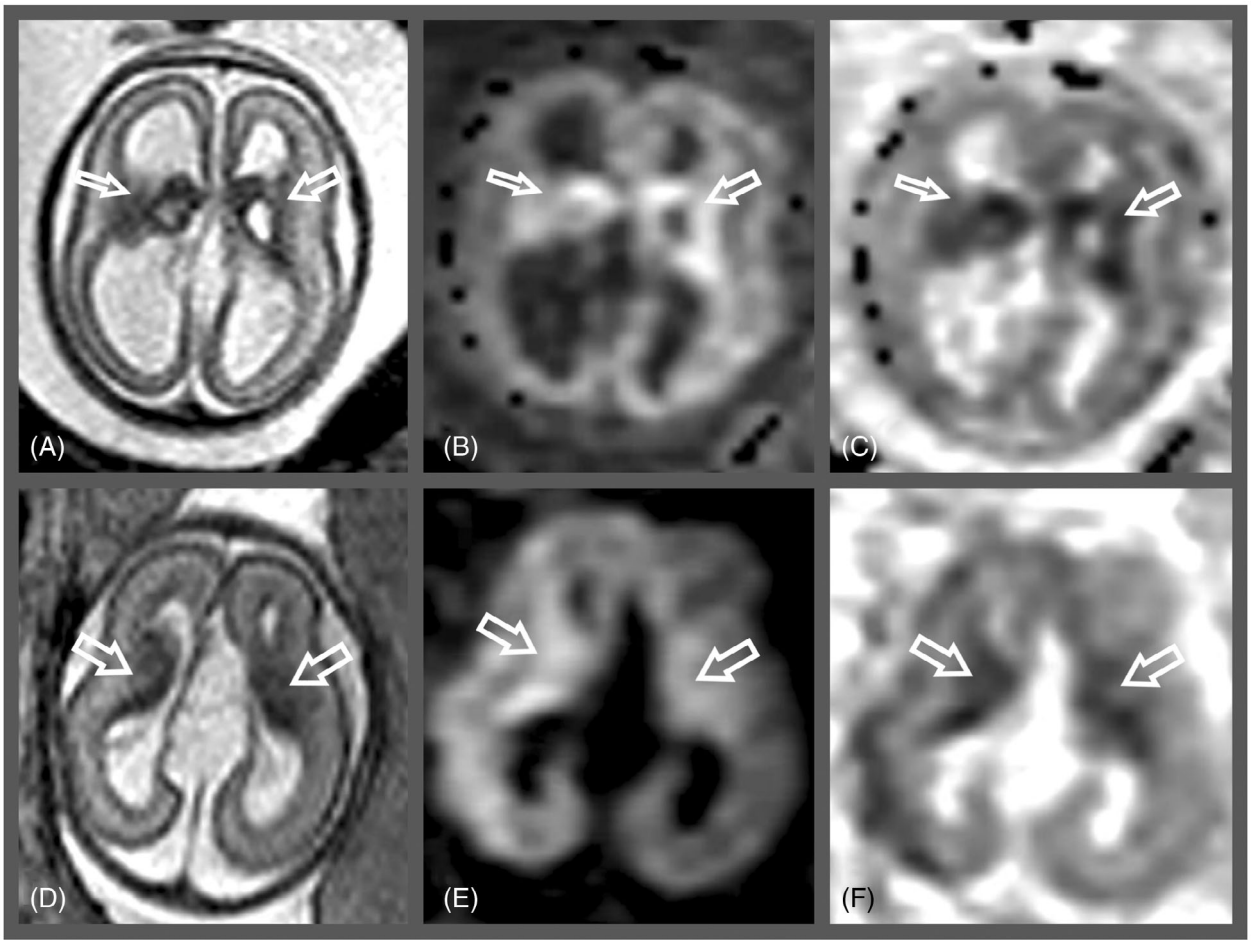

FIGURE 11 Ganglionic eminence abnormalities: (A–C) Cavitations in a 21 GW fetus: (A) axial T2-weighted images and (B) diffusion-weighted image with (C) corresponding ADC map shows bilateral cavitations in the ganglionic eminences surrounded by disorganized, nodular appearance of the surrounding germinal matrix showing restricted diffusion (arrows) due to the increased cellularity. (D, E) Fetus at 21 GW with corpus callosum dysgenesis and an interhemispheric cyst: (D) axial T2-weighted image, (E) diffusion-weighted image, and (F) corresponding ADC map shows bilateral enlargement of the ganglionic eminences, again with restricted diffusion (arrows)

variety of projection neurons and interneurons, prominently including the cortical GABA-ergic interneurons that migrate tangentially to the neocortex.[23,24] A case study from 2021, with more than 300 fetal MRIs included, reported that the GE were visible between 17–30 GW.

The possible abnormalities, which are very rare, can be schematically categorized into two groups, that is, with cavitations or with increased volume[24] (Figure 11). The changes can be bilateral (more commonly) or unilateral and are central to a range of neurodevelopmental abnormalities that encompass abnormal neuroblast proliferation, differentiation, and migration processes, leading to generalized or local abnormal neuronal organization. A strong association between MTOR-PIK3CA (PROS) AKT pathway mutations, including tuberous sclerosis, and fetal head size greater than the 97th centile has been found in patients with GE abnormalities; conversely, TUBA1A mutations were the dominant cause in cases where the frontal-occipital circumference was below the third centile.[25]

The main imaging findings in both types of malformations include restricted diffusion on the DWI sequences in the affected areas, consistent with increased cellular density. The main differential diagnosis includes ischemic and hemorrhagic changes, which give a completely different prognosis to the fetus. In cases of germinal matrix hemorrhage, there will be a signal drop in the T2*/SWI sequences, and the surrounding structures will have a close to normal appearance, in comparison to GE anomalies where they are disorganized and nodular.[24,25]

7 | MALFORMATIONS OF CORTICAL DEVELOPMENT

Cortical development includes several processes, mainly consisting of neuron production, migration, and differentiation. Neocortical progenitor cells arise in the germinal matrix of the ventricular zone and migrate radially along a scaffold consisting of radial glial fibers, forming several migration layers such as the intermediate zone, subplate, and marginal zone. These temporary structures can be visualized during brain development by means of MRI, and can be used as predictive factors for the eventual brain appearance.[23] Generally, however, evaluation of cortical development and its abnormalities is among the most daunting tasks during second-trimester fetal MRI, mostly due to the immature appearance of the brain at this stage and the paucity and subtlety of the findings. The main criteria that can be used include the size of the head and brain, the presence of normal sulcation and gyration, and the expected appearance of the cortical layering at the various gestational weeks.

7.1 | Head and brain size

A normal size of the head and the brain of the fetus does not exclude and underlying pathology, but the presence of micro- or macrocephaly can be used as a criterion for further analysis. Measurements include the skull and brain biparietal diameter (BPD) and frontal-occipital diameter (FOD), that are compared with the normal ranges for the relevant gestational age. Because of the rapidly changing appearances, it is strongly recommended to use previously published reference values.[3]

Microcephaly (Figure 12) is defined as a reduction of the head circumference by at least 2 standard deviations, that is, below the third percentile. It can further be categorized into microcephaly with simplification of the gyral pattern due to impairment of normal neurogenesis or be associated with a wide variety of brain malformations, most prominently lissencephaly spectrum disorders.[26]

Macrocephaly is defined as an increase in head circumference greater than two standard deviations, or above the 97th percentile. MRI is used to distinguish between cases of megalencephaly (abnormal brain overgrowth) and other causes of increased head circumference such as ventriculomegaly, extra-axial space enlargement, congenital tumors, or skeletal dysplasia.[26] Megalencephaly represents a spectrum of cortical malformations caused by either increased neuronal proliferation or a lack of apoptosis. It can be focal or diffuse, uni- or bilateral, and it can be associated with a range of other cortical, midline, or posterior fossa abnormalities.[27] Fetal MRI (Figure 13) shows asymmetry in size of the cerebral hemispheres, cortical abnormalities, and a characteristic straightening of the frontal horns of the

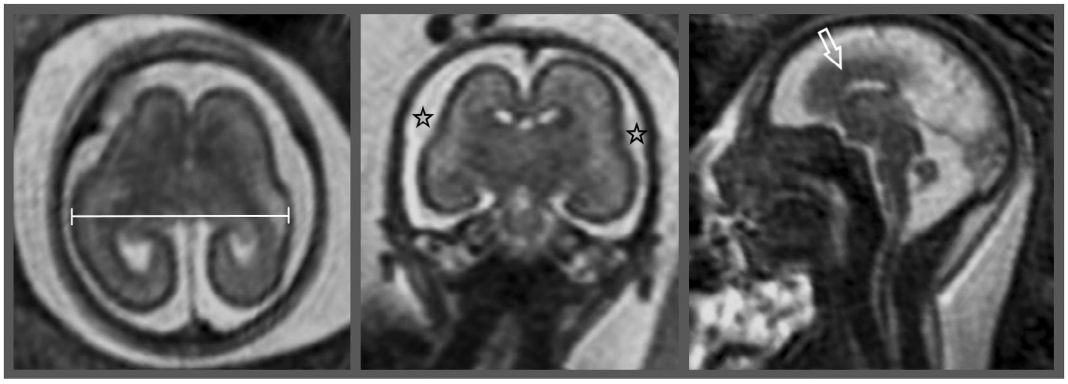

FIGURE 12 Microcephaly, 21 GW. (A) Axial T2-weighted image shows reduced biparietal diameter (line). (B) Coronal T2-weighted image shows flattened, barely visible Sylvian fissures (stars). (C) sagittal T2-weighted image shows hypoplastic corpus callosum (white arrow)

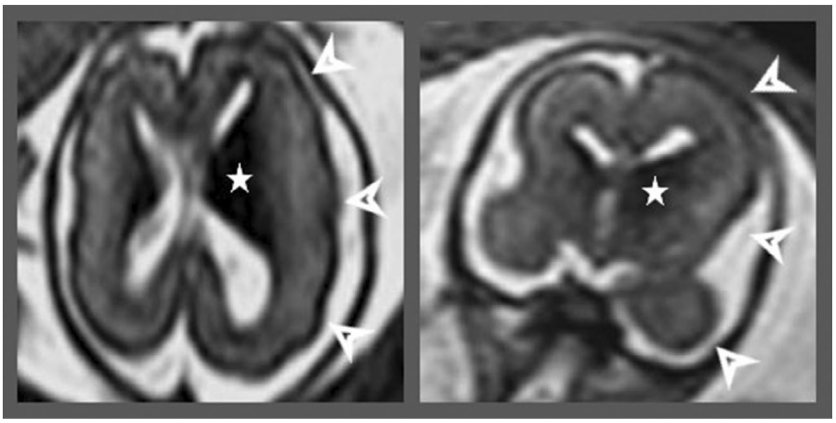

FIGURE 13 Hemimegalencephaly, 21 GW. (A) axial and (B) coronal T2-weighted images show asymmetric enlargement of the left cerebral hemisphere (arrows) and ipsilateral ganglionic eminence (stars). Case courtesy of Andrea Righini, Milan, Italy

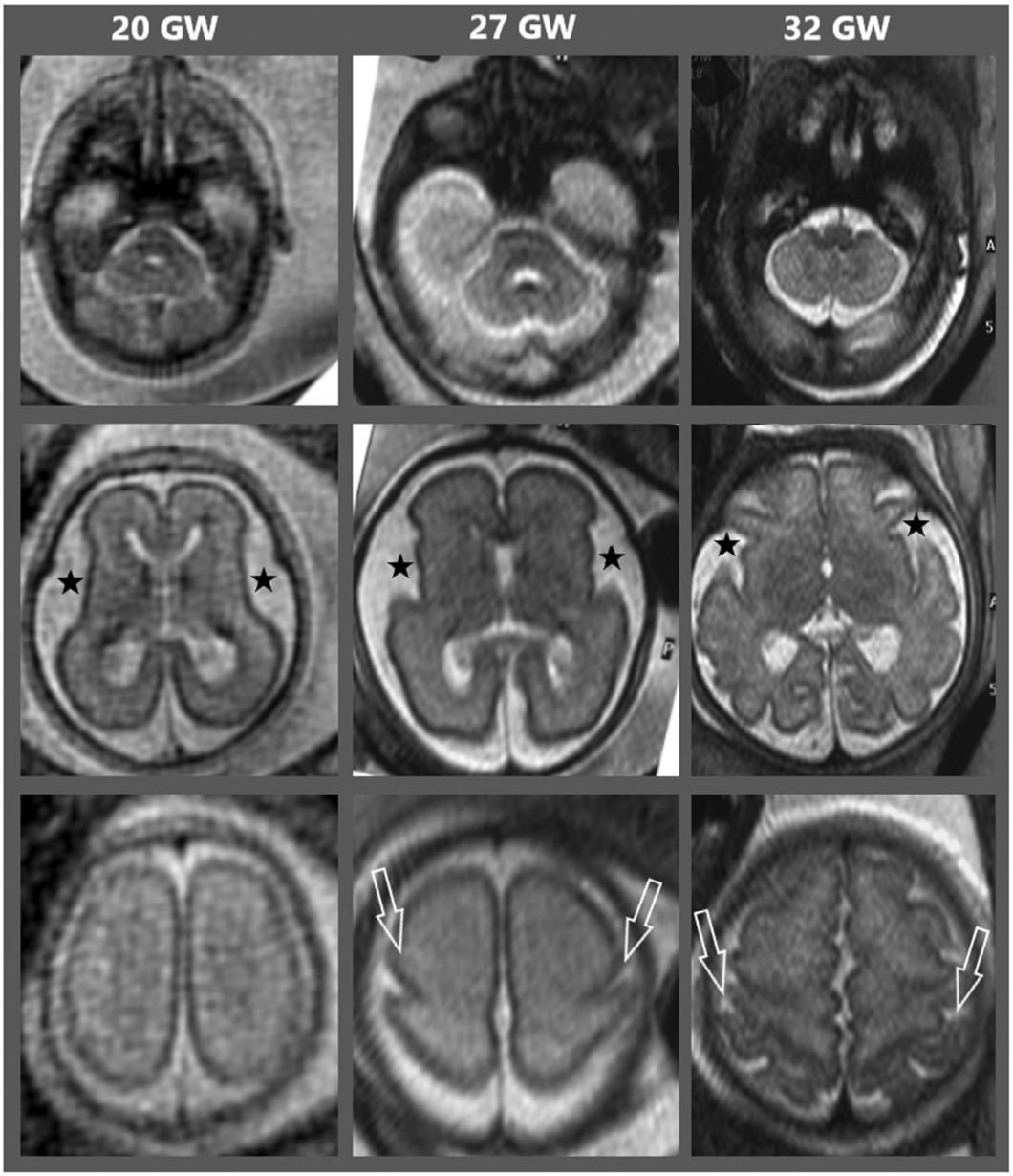

FIGURE 14 Normal dynamic changes of sulcation at various gestational ages (20, 27, and 32 GW). Upper row, development of the cerebellum; middle row, evolution of the Sylvian fissure (black stars) starting from bilateral narrowing with progressive closure due to the enlargement of the surrounding brain; lower row shows progressive appearance of the Rolandic sulcus over the convexity (white arrows)

affected lateral ventricle which is especially helpful to suspect the abnormality early on, when sulcation has yet to appear.[26]

7.2 | Sulcation and gyration

Sulcation is a dynamic process (Figure 14) that begins early in the development of the brain with the formation of the first primary longitudinal fissure, dividing the two cerebral hemispheres. The brain surface is physiologically smooth in the early gestational weeks, followed by primary, secondary, and tertiary sulcation that continues even in the postnatal period. While performing a brain fetal MRI, any sign of asymmetry or deviation from the expected sulcation for the specific age should be carefully evaluated[26,28] (Figure 15). Four major patterns of focal cortical plate abnormalities can be identified before 24 GW: wartlike, sawtooth, abnormal invagination sulcus, and focal bumps (Figures 16 and 17); on follow-up (postnatal, postmortem, or later fetal examination), these were proven to evolve into different types of cortical malformations, most prominently polymicrogyria. Identifying one of those phenotypes, combined with a thinned or blurred subplate and intermediate zone, is highly suggestive of deranged cortical development.[29]

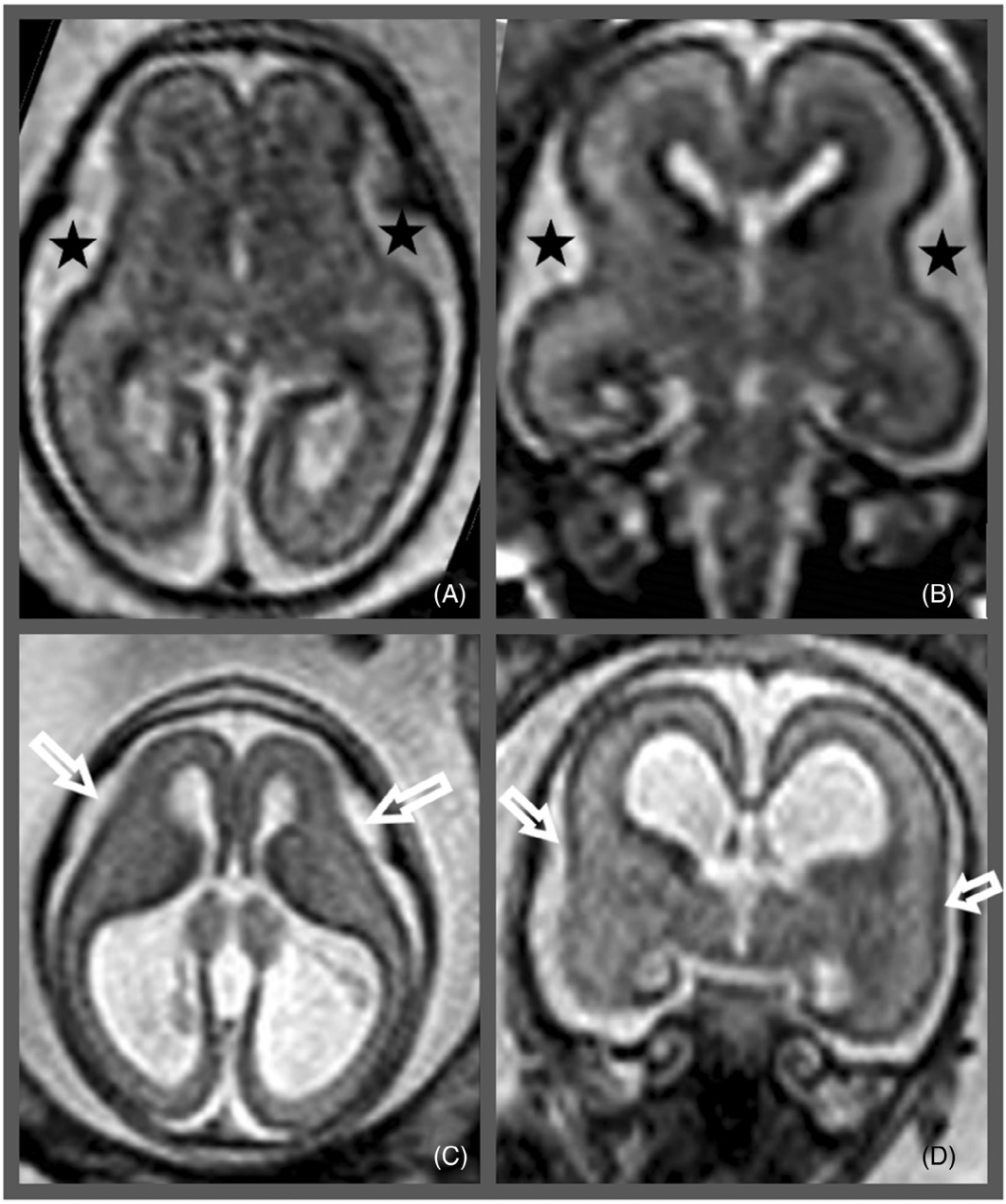

FIGURE 15 Lissencephaly, 21 GW: (A) axial and (B) coronal T2-weighted images in a normal individual shows physiologic appearance of the Sylvian fissures at this age (stars). (C) axial and (D) coronal T2-weighted images in a patient with ventriculomegaly shows absence of primary sulcation with flattening of the fronto-temporal regions (arrows)

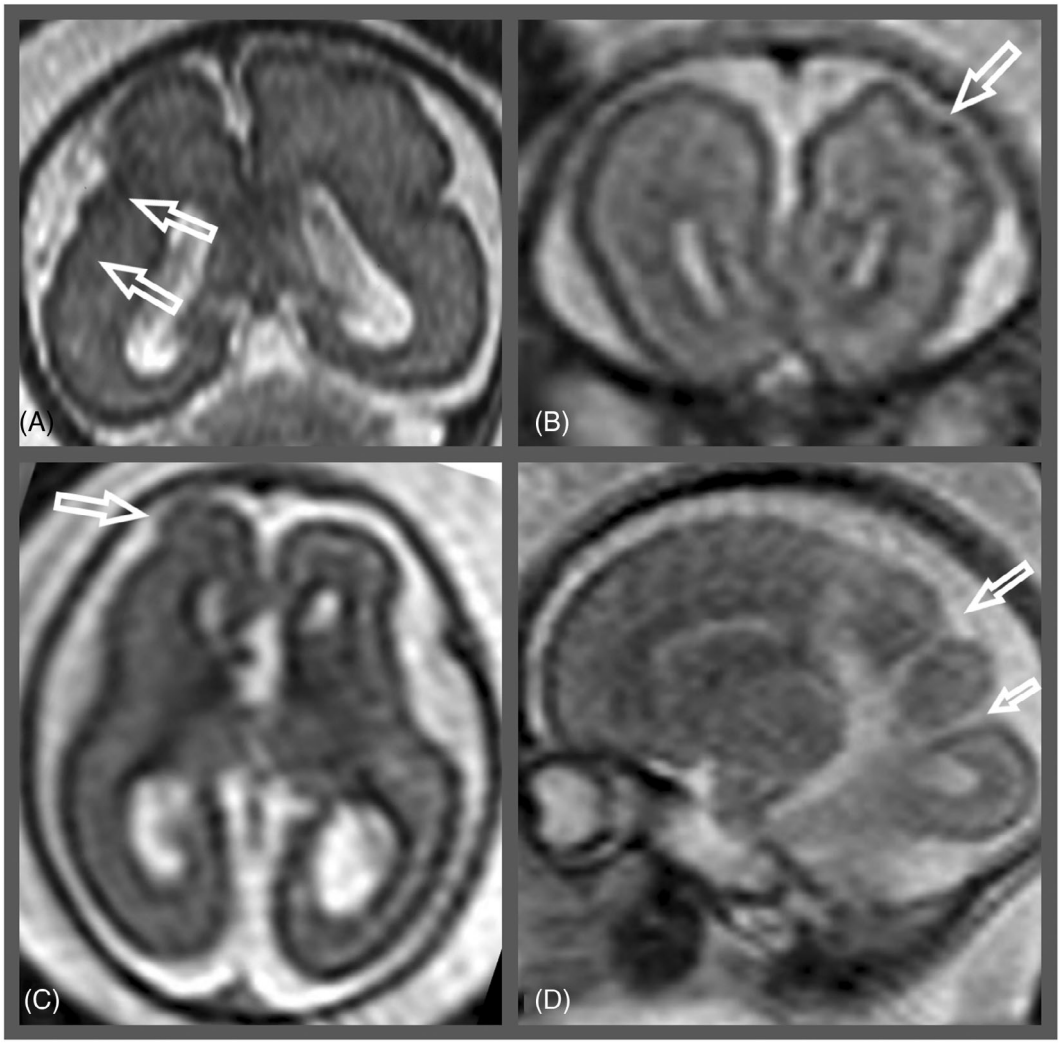

FIGURE 16 Polymicrogyria: different early cortical patterns. (A) coronal T2-weighted image in a 22 GW fetus showing the "sawtooth" appearance (arrows); (B) coronal T2-weighted image in a 22 GW fetus with the "wartlike" pattern (arrow); (C) axial T2-weighted image in a 21 GW fetus showing focal bump in the right frontal lobe (arrow); (D) sagittal T2-weighted image in a 21 GW fetus showing abnormal sulci (arrows) in the parieto-occipital region

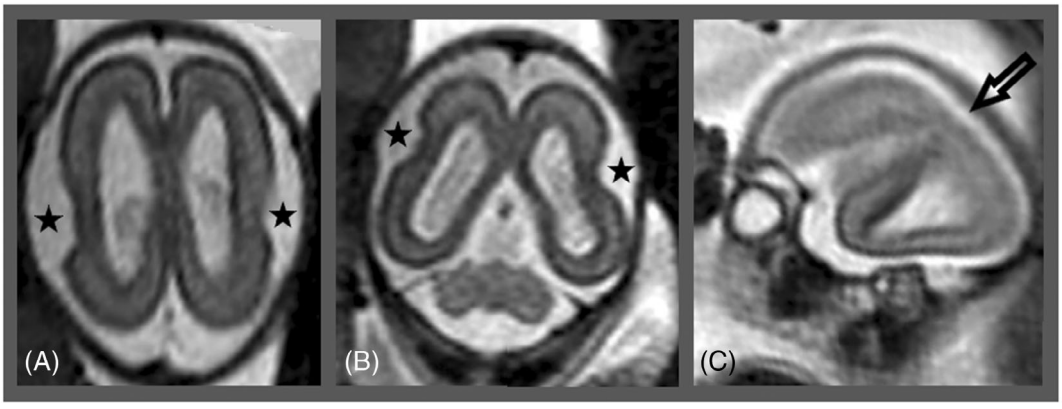

FIGURE 17 Perisylvian polymicrogyria at 21 GW. (A) axial and (B) coronal T2-weighted images show abnormal shape of the Sylvian fissures with abrupt angulations (stars); (C) sagittal T2-weighted image shows continuity between the Sylvian fissure and a convexity sulcus (arrow)

7.3 | Cerebral mantle layering

During normal brain development, the cerebral mantle is composed of temporary concentric layers representing the various stages of the neuronal migration process; in an inside-out fashion, these layers are the germinal zone, the intermediate zone, the subplate, and the cortical plate. The subplate (SP) is the most prominent among these transient layers, existing between 17 and 37 GW, and corresponding to the zone where the neurons, still associated with the radial fibers, are waiting to eventually migrate into their cortical destination.[29] Histologically, SP cells are surrounded by a highly hydrophilic extracellular matrix that can be easily recognized in the T2-weighted images as a hyperintense band between 19 and 23 GW.[30] Visualization of the SP is enhanced on diffusion weighted imaging (DWI; b-values 700 mm^2/s in our practice)[31] (Figure 18) and echo-planar FLAIR,[32] where it lasts longer than in the T2-weighted images, up to 28–30 GW and even later in the temporo-occipital lobes. Evaluating the persistence and integrity of the subplate can be used as an early indicator for interruption of the normal process of neuronal migration that will eventually evolve into cortical malformations (Figure 19).

8 | GRAY MATTER HETEROTOPIA

This malformation involves abnormal locations of normal neuronal clusters and can have various clinical presentations, from asymptomatic to developmental delay and drug-resistant epilepsy. Periventricular nodular heterotopia (PVNH) is the most common type, appearing as gray matter nodules attached to the ventricular wall, varying in size, shape, number, and location. PVNH can be isolated or part of a syndrome or complex brain malformations.[26]

In fetal MRI, PVNH can be observed as an irregularity or focal thickening of the ventricular wall (Figures 20 and 21) but is an elusive finding, especially early in the second trimester (Figure 22). Accuracy of fetal MRI has been reported at 100% in detecting polymicrogyria, schizencephaly, and heterotopia after 24 GW, but such figures drop significantly at earlier gestational ages.[28]

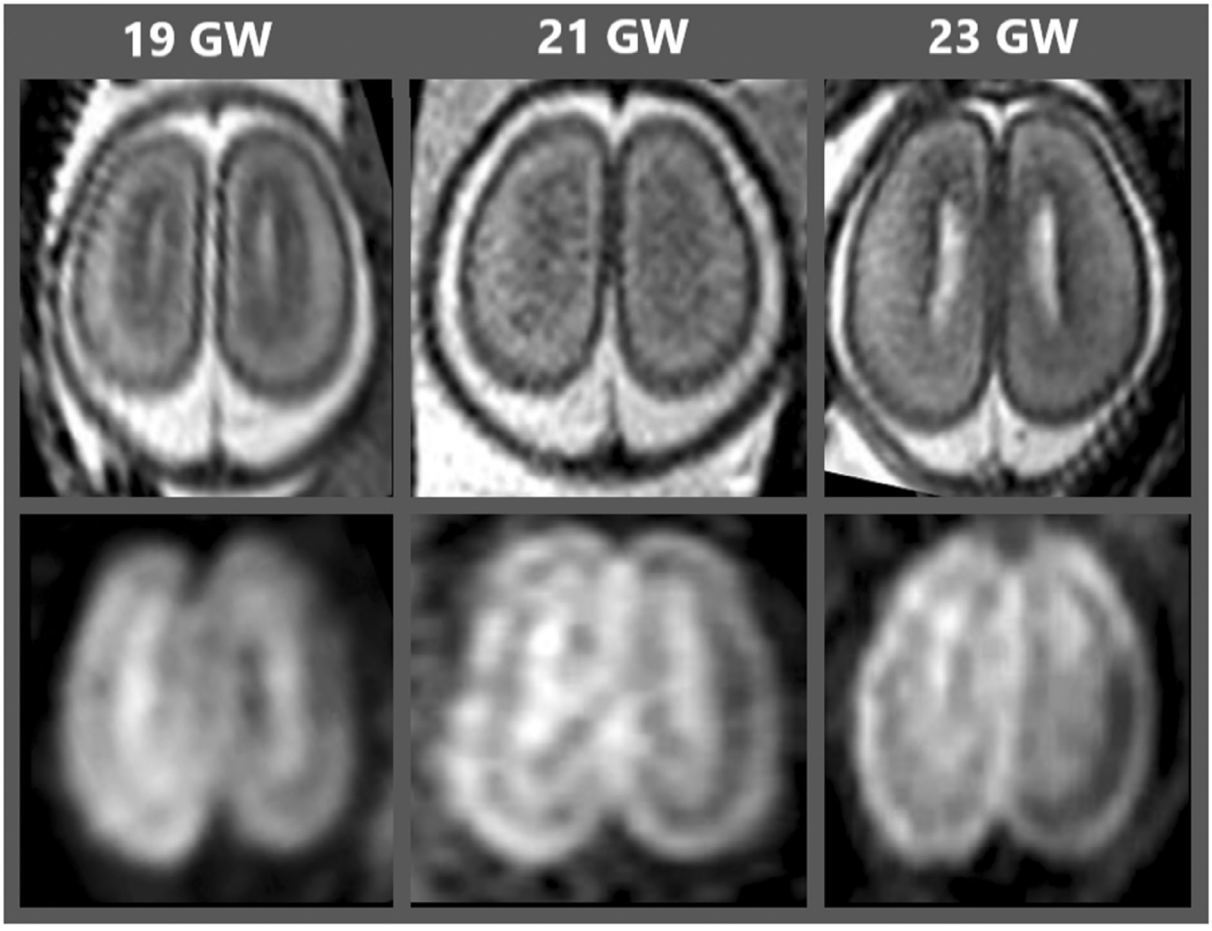

FIGURE 18 Normal cerebral mantle layering on T2 and DWI (b = 700) at different gestational ages (19, 21, and 23 GW). Upper row: axial T2-weighted images reveal subplate as a hyperintense layer subjacent the cortical plate; layering is better seen at 19 GW and almost completely disappeared at 23 GW; lower row, diffusion-weighted images show persistent layering with visibility of the hypointense subplate well into the 23 GW

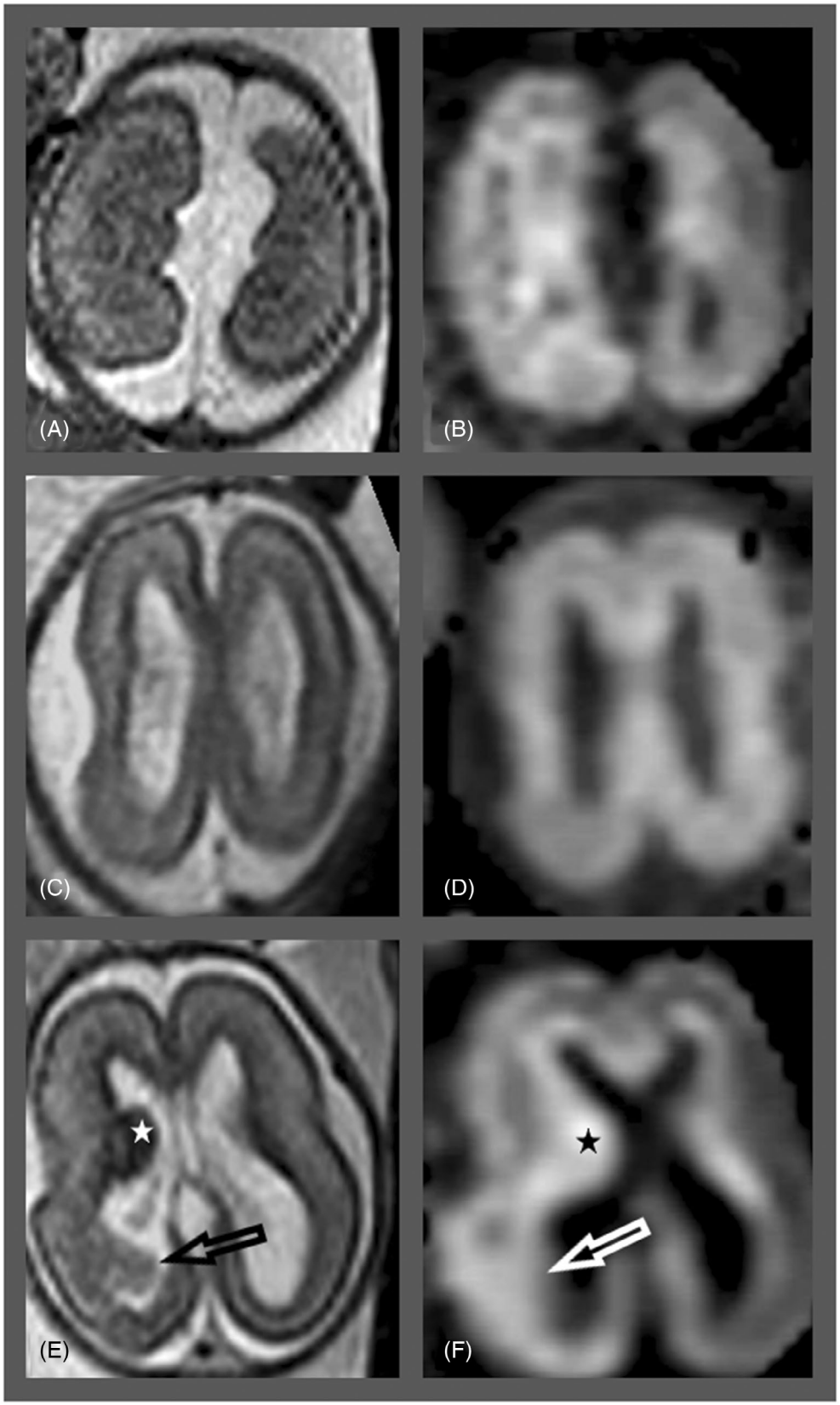

FIGURE 19 Cortical malformations and loss of cerebral mantle layering. (A, B) in this 21 GW fetus with abnormal medial sulcation (A), DWI shows global loss of layering (B). (C, D) Another 21 GW fetus with abnormal shape of the Sylvian fissures (C) and loss of layering on DWI (D). (E, F) Focal nodular area (arrow, E), probably representing subcortical heterotopia, with corresponding loss of layering on DWI (arrow, F). Notice concurrent ganglionic eminence hypertrophy (star, E, F)

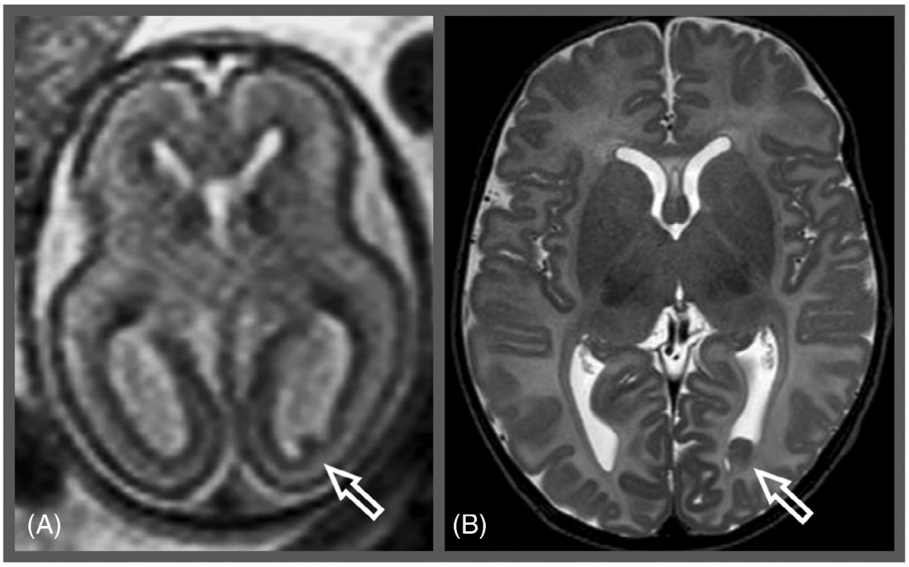

FIGURE 20 Periventricular nodular heterotopia at 21 GW. (A) axial T2-weighted image shows nodular irregularity at the occipital horn of the left lateral ventricle (arrow). (B) postnatal axial T2-weighted image confirms the finding (arrow)

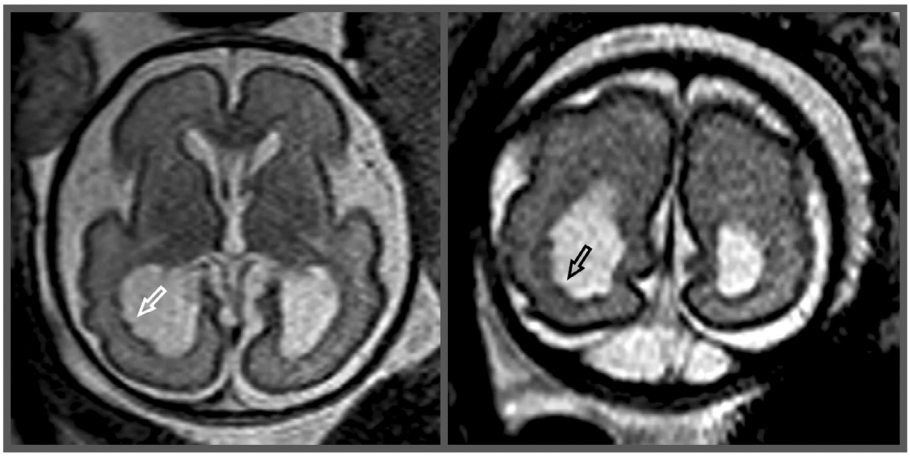

FIGURE 21 Periventricular nodular heterotopia at 24 GW. (A) Axial and (B) coronal T2-weighted images show irregular, string-of-beads appearance of the ependymal margin of the right lateral ventricle (arrowheads) corresponding to multiple heterotopic nodules

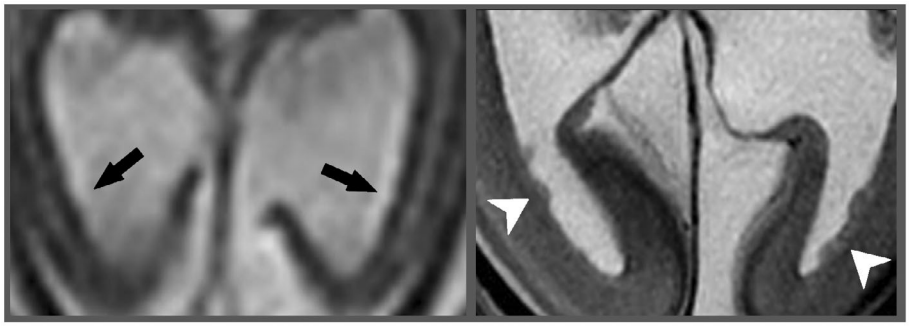

FIGURE 22 Periventricular nodular heterotopia. (A) axial T2-weighted image at 21 GW shows severe ventriculomegaly; notice smooth ependymal walls (arrows) with no evidence of heterotopia. (B) postmortem axial T2-weighted image clearly reveals multiple bilateral heterotopic nodules (arrows)

9 | 1.5 T VERSUS 3 T

Through the years, the superiority of higher magnetic field scanners for brain MR studies has been proven in both adult and pediatric age groups; a similar trend is presently consolidated also for fetal MR imaging. Studies comparing 1.5 and 3 T fetal MRIs revealed that difference in image quality is even more significant at earlier gestational ages such as during the second trimester.[33,34] Despite the improved visualization, the longer acquisition time, which increases the likelihood of motion artifacts, is still regarded as a disadvantage of 3 T scanners. However, it is expected that the use of 3 T will increase soon also for fetal studies, potentially leading to increased diagnostic quality.

10 | CONCLUSIONS

The features of several brain malformations, although rudimentary, can be confidently recognized on second trimester fetal MRI, with potential significant contribution to parental counseling and pregnancy management. Later in pregnancy, follow-up may still be advisable (or even required) in some cases. Diagnoses should be discussed in consensus with the obstetric fetal imaging expert prior to communication with the patient.

ACKNOWLEDGMENT

Open access funding provided by BIBLIOSAN.

DATA AVAILABILITY STATEMENT

The data that support the findings of this study are available from the corresponding author upon reasonable request.

ORCID

Nevena Fileva https://orcid.org/0000-0002-3120-7587
Mariasavina Severino https://orcid.org/0000-0003-4730-5322
Domenico Tortora https://orcid.org/0000-0002-5621-4046
Antonia Ramaglia https://orcid.org/0000-0003-2998-3322
Dario Paladini https://orcid.org/0000-0002-5102-6062
Andrea Rossi https://orcid.org/0000-0001-8575-700X

REFERENCES

1. Lavelanet AF, Schlitt S, Johnson BR Jr, Ganatra B. Global abortion policies database: a descriptive analysis of the legal categories of lawful abortion. *BMC Int Health Hum Rights*. 2018;18(1):44.
2. Dovjak GO, Schmidbauer V, Brugger PC, et al. Normal human brainstem development in vivo: a quantitative fetal MRI study. *Ultrasound Obstet Gynecol*. 2021;58(2):254-263.
3. Conte G, Milani S, Palumbo G, et al. Prenatal brain MR imaging: reference linear biometric centiles between 20 and 24 gestational weeks. *AJNR Am J Neuroradiol*. 2018;39(5):963-967.
4. Krajden Haratz K, Oliveira Szejnfeld P, Govindaswamy M, et al. Prenatal diagnosis of rhombencephalosynapsis: neuroimaging features and severity of vermian anomaly. *Ultrasound Obstet Gynecol*. 2021;58(6):864-874.
5. Sato T, Joyner AL. The duration of Fgf8 isthmic organizer expression is key to patterning different tectal-isthmo-cerebellum structures. *Development*. 2009;136(21):3617-3626.
6. Utsunomiya H, Takano K, Ogasawara T, Hashimoto T, Fukushima T, Okazaki M. Rhombencephalosynapsis: cerebellar embryogenesis. *AJNR Am J Neuroradiol*. 1998;19(3):547-549.
7. Severino M, Huisman T. Posterior fossa malformations. *Neuroimaging Clin N Am*. 2019;29(3):367-383.
8. Ishak GE, Dempsey JC, Shaw DWW, et al. Rhombencephalosynapsis: a hindbrain malformation associated with incomplete separation of midbrain and forebrain, hydrocephalus and a broad spectrum of severity. *Brain*. 2012;135(5):1370-1386.
9. Robinson AJ. Inferior vermian hypoplasia—preconception, misconception. *Ultrasound Obstet Gynecol*. 2014;43(2):123-136.
10. Paladini D, Donarini G, Parodi S, Volpe G, Sglavo G, Fulcheri E. Hindbrain morphometry and choroid plexus position in differential diagnosis of posterior fossa cystic malformations. *Ultrasound Obstet Gynecol*. 2019;54(2):207-214.
11. Pinto J, Paladini D, Severino M, et al. Delayed rotation of the cerebellar vermis: a pitfall in early second-trimester fetal magnetic resonance imaging. *Ultrasound Obstet Gynecol*. 2016;48(1):121-124.
12. Paladini D, Quarantelli M, Pastore G, Sorrentino M, Sglavo G, Nappi C. Abnormal or delayed development of the posterior membranous area of the brain: anatomy, ultrasound diagnosis, natural history and outcome of Blake's pouch cyst in the fetus. *Ultrasound Obstet Gynecol*. 2012;39(3):279-287.
13. Miller E, Orman G, Huisman T. Fetal MRI assessment of posterior fossa anomalies: a review. *J Neuroimaging*. 2021;31(4):620-640.
14. Whitehead MT, Barkovich MJ, Sidpra J, et al. Refining the neuroimaging definition of the Dandy-Walker phenotype. *AJNR Am J Neuroradiol*. 2022;43:1488-1493.
15. Conte G, Caschera L, Parazzini C, et al. Prenatal magnetic resonance imaging within the 26th week of gestation may predict the fate of isolated upward rotation of the cerebellar vermis: insights from a multicentre study. *Eur Radiol*. 2020;30(4):2161-2170.
16. Whitehead MT, Vezina G, Schlatterer SD, Mulkey SB, du Plessis AJ. Taenia-Tela choroidea complex and choroid plexus location help distinguish Dandy-Walker malformation and Blake pouch cysts. *Pediatr Radiol*. 2021;51(8):1457-1470.
17. Mitchison HM, Valente EM. Motile and non-motile cilia in human pathology: from function to phenotypes. *J Pathol*. 2017;241(2):294-309.
18. Romani M, Micalizzi A, Valente EM. Joubert syndrome: congenital cerebellar ataxia with the molar tooth. *Lancet Neurol*. 2013;12(9):894-905.
19. Lerman-Sagie T, Prayer D, Stöcklein S, Malinger G. Fetal cerebellar disorders. *Handb Clin Neurol*. 2018;155:3-23.
20. Severino M, Tortora D, Pistorio A, et al. Expanding the spectrum of congenital anomalies of the diencephalic-mesencephalic junction. *Neuroradiology*. 2016;58(1):33-44.
21. Severino M, Righini A, Tortora D, et al. MR imaging diagnosis of diencephalic-mesencephalic junction dysplasia in fetuses with developmental ventriculomegaly. *AJNR Am J Neuroradiol*. 2017;38(8):1643-1646.
22. Accogli A, Goergen S, Izzo G, et al. L1CAM variants cause two distinct imaging phenotypes on fetal MRI. *Ann Clin Transl Neurol*. 2021;8(10):2004-2012.
23. Stiles J, Jernigan TL. The basics of brain development. *Neuropsychol Rev*. 2010;20(4):327-348.
24. Scarabello M, Righini A, Severino M, et al. Ganglionic Eminence anomalies and coexisting cerebral developmental anomalies on fetal MR imaging: multicenter-based review of 60 cases. *AJNR Am J Neuroradiol*. 2021;42(6):1151-1156.
25. Goergen SK, Alibrahim E, Christie J, et al. The fetus with ganglionic Eminence abnormality: head size and extracranial sonographic findings predict genetic diagnoses and postnatal outcomes. *AJNR Am J Neuroradiol*. 2021;42(8):1528-1534.
26. Severino M, Geraldo AF, Utz N, et al. Definitions and classification of malformations of cortical development: practical guidelines. *Brain*. 2020;143(10):2874-2894.
27. Accogli A, Geraldo AF, Piccolo G, et al. Diagnostic approach to macrocephaly in children. *Front Pediatr*. 2021;9:794069.
28. Glenn OA, Cuneo AA, Barkovich AJ, Hashemi Z, Bartha AI, Xu D. Malformations of cortical development: diagnostic accuracy of fetal MR imaging. *Radiology*. 2012;263(3):843-855.
29. Righini A, Parazzini C, Doneda C, et al. Early formative stage of human focal cortical gyration anomalies: fetal MRI. *AJR Am J Roentgenol*. 2012;198(2):439-447.
30. Perkins L, Hughes E, Srinivasan L, et al. Exploring cortical subplate evolution using magnetic resonance imaging of the fetal brain. *Dev Neurosci*. 2008;30(1-3):211-220.
31. Kasprian G, Del Rio M, Prayer D. Fetal diffusion imaging: pearls and solutions. *Top Magn Reson Imaging*. 2010;21(6):387-394.
32. Diogo MC, Prayer D, Gruber GM, et al. Echo-planar FLAIR sequence improves subplate visualization in fetal MRI of the brain. *Radiology*. 2019;292(1):159-169.

33. da Silva NA Jr, Vassallo J, Sarian LO, Cognard C, Sevely A. Magnetic resonance imaging of the fetal brain at 3 tesla: preliminary experience from a single series. *Medicine (Baltimore)*. 2018;97(40):e12602.
34. Victoria T, Johnson AM, Edgar JC, Zarnow DM, Vossough A, Jaramillo D. Comparison between 1.5-T and 3-T MRI for fetal imaging: is there an advantage to imaging with a higher field strength? *Am J Roentgenol*. 2016;206(1):195-201.

How to cite this article: Fileva N, Severino M, Tortora D, Ramaglia A, Paladini D, Rossi A. Second trimester fetal MRI of the brain: Through the ground glass. *J Clin Ultrasound*. 2023; 51(2):283-299. doi:10.1002/jcu.23423